Ion concentrations and velocity profiles in nanochannel electroosmotic flows

R. Qiao and N. R. Aluru[a)]
Beckman Institute for Advanced Science and Technology, University of Illinois at Urbana-Champaign, Urbana, Illinois 61801

(Received 12 August 2002; accepted 11 December 2002)

Ion distributions and velocity profiles for electroosmotic flow in nanochannels of different widths are studied in this paper using molecular dynamics and continuum theory. For the various channel widths studied in this paper, the ion distribution near the channel wall is strongly influenced by the finite size of the ions and the discreteness of the solvent molecules. The classical Poisson–Boltzmann equation fails to predict the ion distribution near the channel wall as it does not account for the molecular aspects of the ion–wall and ion–solvent interactions. A modified Poisson–Boltzmann equation based on electrochemical potential correction is introduced to account for ion–wall and ion–solvent interactions. The electrochemical potential correction term is extracted from the ion distribution in a smaller channel using molecular dynamics. Using the electrochemical potential correction term extracted from molecular dynamics (MD) simulation of electroosmotic flow in a 2.22 nm channel, the modified Poisson–Boltzmann equation predicts the ion distribution in larger channel widths (e.g., 3.49 and 10.00 nm) with good accuracy. Detailed studies on the velocity profile in electro-osmotic flow indicate that the continuum flow theory can be used to predict bulk fluid flow in channels as small as 2.22 nm provided that the viscosity variation near the channel wall is taken into account. We propose a technique to embed the velocity near the channel wall obtained from MD simulation of electroosmotic flow in a narrow channel (e.g., 2.22 nm wide channel) into simulation of electroosmotic flow in larger channels. Simulation results indicate that such an approach can predict the velocity profile in larger channels (e.g., 3.49 and 10.00 nm) very well. Finally, simulation of electroosmotic flow in a 0.95 nm channel indicates that viscosity cannot be described by a local, linear constitutive relationship that the continuum flow theory is built upon and thus the continuum flow theory is not applicable for electroosmotic flow in such small channels.
 [DOI: 10.1063/1.1543140]

I. INTRODUCTION

With the growing interest in bio-MEMS (Micro-Electro-Mechanical-Systems) and bio-NEMS (Nano-Electro-Mechanical-Systems) applications, as well as in fuel cell technologies, electroosmotic transport has attracted considerable attention in recent years.[1–5] Electroosmotic transport[6] is easy to control and usually scales more favorably compared to other fluidic transport methods (e.g., a pressure driven flow) at micro- and nanoscales. Modeling and simulation of electroosmotic transport, based on the classical Poisson–Boltzmann equation and the Navier–Stokes equations, has explained many experimental observations and guided the design of μ-TAS (micro-Total-Analysis-Systems).[7–10] There is now a growing interest in developing nanoscale fluidic systems that can be used to manipulate molecular level transport. For example, nanofluidic systems can enable the molecular separation and identification of analytes at an unprecedented low level of sample volumes.[3,11] Modeling and simulation of electrically mediated fluid flow in nanometer wide channels can address many of the fundamental issues currently facing the design of nanofluidic systems.[11]

A fundamental issue that needs to be addressed is whether or not continuum theories based on the Poisson–Boltzmann and the Navier–Stokes equations—that have been popularly used to understand electroosmotic flow in micron-scale channels—can be used to describe electroosmotic flow in nanometer wide channels. In nanoscale systems, the surface-to-volume ratio is very high and the critical dimension is comparable to the size of the molecules. The influence of the surface and the finite-size effect of the molecule on ion distributions and fluid flow in nanoscale channels needs to be understood in detail while such effects may be largely neglected in microscale channels. For example, in the derivation of the classical Poisson–Boltzmann equation, the ions are assumed to be infinitesimal, the interactions between the ions, ion–water and ion–wall are all considered in a mean-field fashion and the molecular aspects of these interactions are neglected. Similarly, the continuum flow theory based on Stokes or Navier–Stokes equations assumes that the state variables (e.g., density) do not vary significantly over intermolecular distances and the shear stress can be related to the local strain rate by a linear constitutive relationship. However, significant fluctuations in fluid density have been observed close to the surface in molecular dynamics simulations[12] as well as in experiments.[13] Earlier

[a]Electronic address: aluru@uiuc.edu;
URL: http://www.staff.uiuc.edu/~aluru

studies on Poiseuille flow of Lennard-Jones atoms indicated that the continuum theory breaks down for channels narrower than four molecular diameters.[12] Hence, it is important to understand in detail the validity of continuum theories for electroosmotic fluid flow in nanometer wide channels.

Molecular dynamics (MD) simulation is an important tool to study fluid flow in nanometer wide channels. In a MD simulation, the molecular interactions between ion–ion, ion–wall, and ion–water are calculated explicitly by using the Coulomb potential and the Lennard-Jones potential. The Lennard-Jones potential is an empirical potential that parameterizes a number of different molecular interactions (e.g., the van der Waals interaction is mainly described by the attractive part of the Lennard-Jones potential). Since the ion–ion, ion–wall, and ion–water interactions are treated only in a mean-field fashion in the classical continuum theory, the significance of the molecular aspects of these interactions can be understood by a detailed comparison between MD and continuum results. Molecular dynamics simulation of electroosmotic flow in a 6.53 nm wide channel has been reported recently and ion distributions from molecular dynamics have been found to be different from those predicted by the classical Poisson–Boltzmann theory.[14] In addition, it was also reported that the shear viscosity near the channel wall increases dramatically.[14]

In this paper we study electroosmotic transport in nanochannels with widths ranging from 0.95 to 10.00 nm using molecular dynamics and continuum theory. Section II describes the continuum modeling approach for electroosmotic flow, Sec. III describes the simulation of electroosmotic flow using nonequilibrium molecular dynamics (NEMD) technique, and Sec. IV presents results on ion distributions in various nanometer wide channels by comparing continuum and molecular dynamics results. The significance of molecular interactions between ion–wall and ion–water are discussed in detail for different cases. A modified Poisson–Boltzmann equation, which incorporates the various molecular interactions in a lumped manner, is also presented in Sec. IV. Section V presents results on velocity profiles for various channel widths by comparing continuum theory and molecular dynamics results. A technique that embeds MD velocity data from a smaller length scale into simulation of electroosmotic flow in larger width channels is also presented in Sec. V. Finally, conclusions are presented in Sec. VI.

II. CONTINUUM MODELING OF ELECTROOSMOTIC FLOW

In this paper, we focus on the study of electroosmotic transport in straight flat channels (the channel width is in the z-direction, and the flow is along the x-direction, see Fig. 1) where (1) only counter-ions are present in the channel and (2) the flow is fully-developed and there is no externally applied pressure gradient. For electroosmotic transport in a straight flat channel with uniform charge densities on the channel walls and filled with water and single mobile ion species, the continuum mathematical description is based on the Poisson–Boltzmann equation (1) and the Stokes equation (2)

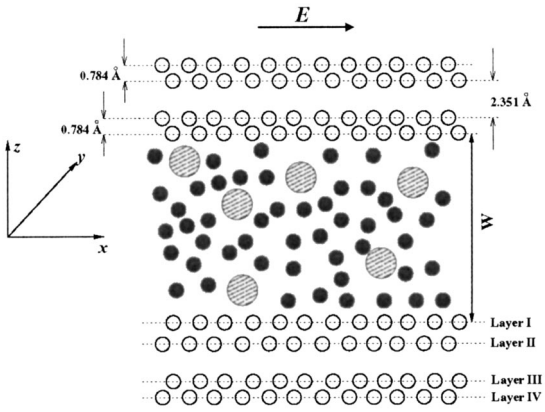

FIG. 1. A schematic of the channel system under investigation. The two channel walls are symmetrical with respect to the channel center line. Each wall is made up of four layers of silicon atoms. The channel width W is defined as the distance between the two innermost wall layers. The dark dots denote water molecules and the shaded circles denote either Cl^- or Na^+ ions. For the coordinate system chosen, $z=0$ corresponds to the central plane of the channel system.

$$\frac{\partial^2 \psi(z)}{\partial z^2} = -\frac{q}{\epsilon}\tilde{z}c_0 e^{-q\tilde{z}\psi(z)/k_B T}, \tag{1}$$

$$\frac{d}{dz}\left(\mu \frac{du(z)}{dz}\right) + q\tilde{z}c(z)E_{\text{ext}} = 0, \tag{2}$$

where $\psi(z)$ is the potential induced by the charges on the channel wall and ions in the channel, q is the electron charge (i.e., 1.6×10^{-19} C), $\tilde{z}$ is the valency of the counter-ion, c_0 is the counter-ion concentration at the channel center where the potential is assumed to be zero, ϵ is the permittivity of the fluid in the channel, k_B is the Boltzmann constant, T is the temperature, $u(z)$ is the velocity of the fluid, μ is the dynamic viscosity of the fluid, $c(z)$ is the counter-ion concentration across the channel, and E_{ext} is the external electric field applied along the channel.

The boundary conditions for Eqs. (1) and (2) are

$$\left.\frac{d\psi(z)}{dz}\right|_{z=\pm h/2} = \frac{\sigma_s}{\epsilon}, \tag{3}$$

$$u(z)|_{z=\pm h/2} = 0, \tag{4}$$

where $z=\pm h/2$ corresponds to the location of the lower and the upper channel wall and σ_s is the charge density on the channel walls. Analytical solutions for Eqs. (1) and (2) are available for the boundary conditions given in Eqs. (3) and (4).[15,16] But to use the analytical solution, one needs to first solve a transcendental equation numerically, so Eqs. (1) and (2) are solved numerically in this paper.

The relative permittivity of water is taken as 81, which is the reported value for SPC/E water at 300 K.[17] We note that relative permittivity of water in the channel could be different from its bulk value due to confinement and high electric field near the channel wall.[18,19] However, it was recently reported[14] that the influence of relative permittivity variation in the channel on the ion distribution is less important compared to the ion–wall interactions. Therefore, the relative permittivity is taken as a constant in the entire channel in this

paper. The dynamic viscosity of water is taken as 0.743 mPa s in our continuum simulations because this gives the best match to the velocity profile in the central portion of the channel. We have simulated Poiseuille flow of pure SPC/E water at a peak strain rate of $4.7\times10^{10}\,s^{-1}$, temperature of 300 K, and the dynamic viscosity of water was determined to be 0.683 mPa s, which is within 5% of the reported value for SPC/E water.[20] For an ionic solution, using a viscosity higher than that of pure water is in accordance with the experimental observations that the viscosity of an electrolyte solution increases as the concentration of electrolyte increases. For example, the viscosity of 0.89 M NaCl solution at 293 K is about 8.5% higher than that of pure water at 293 K.[21]

TABLE I. Parameters for the Lennard-Jones potential $U(r)=C_{12}/r^{12}-C_6/r^6$.

Interaction	C_6 (kJ nm^6/mol))	C_{12} (kJ nm^{12}/mol)	σ(nm)[a]
O–O	0.2617×10^{-2}	0.2633×10^{-5}	0.317
O–Si	0.6211×10^{-2}	0.7644×10^{-5}	0.327
O–Cl	0.6011×10^{-2}	0.1678×10^{-4}	0.375
O–Na	0.4343×10^{-3}	0.2352×10^{-6}	0.286
Cl–Cl	0.1380×10^{-1}	0.1069×10^{-3}	0.445
Cl–Si	0.1426×10^{-1}	0.4871×10^{-4}	0.388
Cl–Na	0.9974×10^{-3}	0.1499×10^{-5}	0.339
Na–Na	0.7206×10^{-4}	0.2101×10^{-7}	0.257
Na–Si	0.1031×10^{-2}	0.6829×10^{-6}	0.295

[a]σ is the separation distance between atoms where the potential energy is zero.

III. MOLECULAR DYNAMICS SIMULATION DETAILS

A. Simulated system

NEMD simulations were performed for systems consisting of a slab of water molecules and ions sandwiched by two channel walls. Figure 1 shows a schematic diagram of the system under investigation. The two channel walls are symmetrical with respect to the channel center line. Each wall is made up of four layers of silicon atoms oriented in the $\langle111\rangle$ direction. Typical lateral dimensions of the channel wall are 4.66×4.43 nm which corresponds to 161 silicon atoms for each layer of the channel wall. The channel width is varied from 0.95 to 10.0 nm in the simulations.

For the simulation of electroosmotic flow, the outermost wall layers (i.e., layer I of the lower channel wall and its counterpart in the upper channel wall) are partially charged. In this paper, we will assume that the charges are uniformly distributed among the wall atoms, i.e., wall atoms are partially charged. Previous results on MD simulation of electroosmotic flow show that the flow characteristics are not altered significantly whether the charge is uniformly distributed or discretely distributed.[14] The wall atoms are fixed to their original positions during the simulation. The water is modeled by using the SPC/E model,[22] i.e., water molecule is rigid, and hydrogen and oxygen atoms are modeled as point charges. In the simulation, we consider two types of interaction potentials, i.e., Lennard-Jones and Coulomb potential. The Lennard-Jones potential is considered for every atom pair (except the atom pairs that have hydrogen atom and the Si–Si pair). The parameters for the Lennard-Jones potential are taken from the Gromacs force field[23] and are summarized in Table I. The Coulomb potential is considered for every charged atom pair. In our simulation, the total charge from the counter-ions matches the wall charge exactly, i.e., the system is electrically neutral. Lo *et al.* has shown that for slit pores as small as two ion diameters, the system's deviation from electroneutrality is negligible.[24]

B. NEMD technique

NEMD simulations were performed using a molecular dynamics package Gromacs.[25,26] The equations of motion were integrated using a leap-frog algorithm with a time step ranging from 1.0 to 2.0 fs. A cutoff radius of 1.1 nm was used to compute the Lennard-Jones potential. The electrostatic interactions were computed using the particle mesh Ewald (PME) method[27] with no truncation for the Coulomb interactions. The original PME technique assumes periodicity in all three directions. However, there is no periodicity in the channel width direction (*z*-direction, see Fig. 1) in our channel system. To compute the electrostatic interactions in our system with reduced periodicity, we have (i) modified the original PME algorithm by adding a correction term to the standard Ewald summation formula,[28] and (ii) elongated the simulation box in the *z*-direction to be three times larger than the channel width. A cutoff distance of 1.10 nm was used in the calculation of electrostatic interactions in the real space. An FFT grid spacing of 0.11 nm and cubic interpolation for charge distribution were chosen to compute the electrostatic interactions in the reciprocal space. A LINCS algorithm[29] was used to maintain the water geometry specified by the SPC/E model. The temperature of fluid is regulated to 300 K by using a Berendsen thermostat with a time constant of 0.1 ps. Applying the thermostat to our system was difficult because of a nonzero streaming velocity along the channel. In a rigorous sense, one should distinguish the streaming kinetic energy from the thermal kinetic energy in applying the thermostat. However, the kinetic energy associated with the streaming velocity is only a very small fraction of the thermal kinetic energy (e.g., for a water molecule with a streaming velocity of 25 m/s, the associated kinetic energy is only 0.15% of its thermal kinetic energy at 300 K). Hence, we did not distinguish the thermal kinetic energy from the streaming kinetic energy when applying the thermostat.

When setting up the simulation, the molecules were randomly positioned. An energy minimization was performed to remove the local contacts. To start the simulation, an initial velocity sampled from a Maxwellian distribution at 300 K was assigned to each molecule in the system. The system was simulated for a time period of 1–2 ns so that the system has reached steady state. A production run of 1 to 7 ns (depending on the system to be simulated) was performed to gather the statistics of various quantities, e.g., streaming velocity. The density and velocity profile across the channel were computed by using the binning method.[30] The flow is driven by an external electric field, E_{ext}, applied along the channel in the *x*-direction. Because of the extremely high thermal noise, a strong electric field was applied in our simulations so that the fluid velocity can be retrieved with reasonable accuracy. The external electric field strength used in our

TABLE II. Summary of the simulations performed.

Case #	Channel width (nm)	σ_s (C/m^2)	# Water molecules	# Ions	E_{ext} (V/nm)	Simulation time (ns)
1	3.49	+0.120	2246	32 (Cl^-)	−0.55	5.1
2	3.49	+0.320	2075	85 (Cl^-)	−0.55	2.5
3	3.49	−0.120	2246	32 (Na^+)	+0.55	2.8
4	2.22	+0.120	1288	32 (Cl^-)	−0.46	6.3
5	0.95	+0.120	405	32 (Cl^-)	−0.55	9.4
6	10.00	+0.124	6606	32 (Cl^-)	−0.38	4.8

simulations ranges from 0.38 to 0.55 V/nm. Table II summarizes the various simulations performed in this paper.

IV. ION DISTRIBUTIONS IN ELECTROOSMOTIC FLOW

A. Comparison of continuum and MD simulation results

Figure 2(a) shows the concentration profile of Cl^- ion and water across the channel for case 1, where the channel width is 3.49 nm and the wall charge density is +0.120 C/m^2. The ion distribution obtained from the Poisson–Boltzmann equation is also shown for comparison. To compute the ion distribution using the Poisson–Boltzmann equation, we have assumed that the position of the wall coincides with the position of the first peak of Cl^- ion concentration obtained from MD simulation. The MD simulation result deviates from the Poisson–Boltzmann equation prediction in several aspects: (1) There is no Cl^- ion within 0.24 nm from the channel wall, (2) the peak concentration of Cl^- ion occurs at a position of about 0.35 nm away from the channel wall and the peak value is about 88% higher compared to the P–B equation prediction, and (3) the ion concentration from MD does not decrease monotonically to its value in the channel center. In particular, there is a plateau located at about 0.49–0.60 nm away from the channel wall.

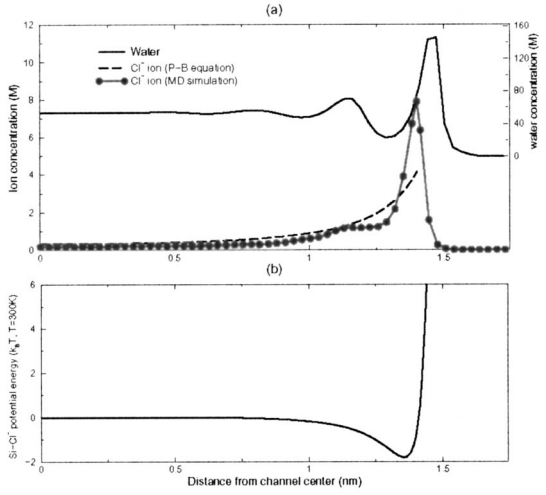

FIG. 2. (a) Cl^- ion and water concentration across the channel for case 1 ($W=3.49$ nm, $\sigma_s=+0.120$ C/m^2). The channel center is located at $z=0$ nm and the position of water molecule is computed as the center-of-mass position. (b) Potential energy of Cl^- ion over the channel wall computed using Lennard-Jones potential. It is assumed that the ion can access any position in the xy-plane with equal probability.

These deviations can be understood by looking at the molecular aspects of the ions, wall atoms and the water molecules. First, since a bare Cl^- ion has an effective radius of about 0.18 nm,[15] a Cl^- ion cannot approach too close to the channel wall. Second, the ion and the wall interact with each other via the Lennard-Jones potential in the MD simulation. Such an interaction can contribute to the attraction of ions towards the wall. Figure 2(b) shows the potential energy of a Cl^- ion due to the Lennard-Jones potential between the Cl^- ion and the channel wall. In this calculation, we have assumed that the ion can access any position in the xy-plane with equal probability. Figure 2(b) indicates that the potential energy due to the ion–wall Lennard-Jones interaction is about $-1.8\,k_BT$ ($T=300$ K) at a position of about 0.39 nm away from the channel wall. Since a location with lower potential energy is more favorable for the ions, the potential energy valley can attract more ions towards it. The second deviation is primarily caused by this effect. Third, the molecular interaction between the ion and the water molecules also plays an important role in determining the ion concentration. Figure 2(a) shows that the water concentration is not uniform across the channel and a significant layering of water is observed near the channel wall. Such a layering effect is well-known and several papers have addressed this issue.[14,15] Since the water molecules are less closely packed near the density ''valley'' than in the bulk, the energy required to insert a finite-sized ion into the density ''valley'' is lower compared to inserting an ion in the bulk. Hence, more ions are attracted towards the density ''valley'' of water. In fact, a very weak peak of Cl^- ion is observed near the second density valley of water. From these results we can infer

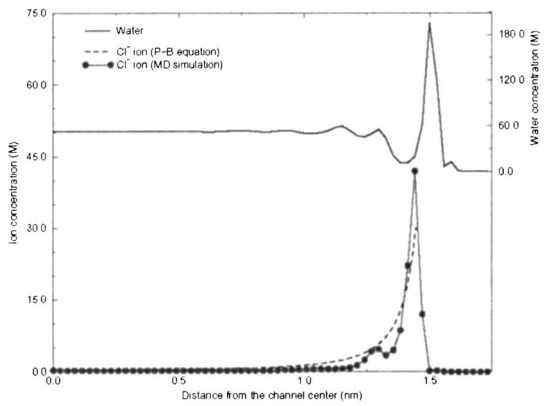

FIG. 3. Cl^- ion and water concentration profile across the channel for case 2 ($W=3.49$ nm, $\sigma_s=+0.320$ C/m^2).

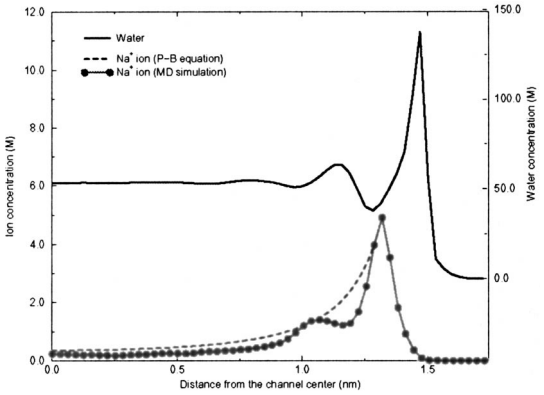

FIG. 4. Na^+ ion and water concentration across the channel for case 3 ($W=3.49$ nm, $\sigma_s=-0.120$ C/m^2).

that the molecular interactions between ion–wall and ion–water play an important role in determining the distribution of ions near the channel wall.

Figure 3 shows the concentration profile of Cl^- ion across the channel for case 2, where the channel width is 3.49 nm and the charge density on the channel wall is $+0.320$ C/m^2. Compared to the previous case, the charge density on the channel wall is very high (such a high charge density is realistic in practical systems[31]). The Poisson–Boltzmann equation again underestimates the ion concentration near the channel wall. A clear second peak of Cl^- concentration is observed at a position of about 0.45 nm away from the channel wall, whereas such a peak was very weak in case 1. The second peak is primarily caused by the fact that the ions are very densely packed (as indicated by the high concentration) near the channel wall and the strong electrostatic repulsion between the ions makes it difficult to accommodate more ions in the region within 0.41 nm from the channel wall. As a result, a second peak is observed. Since the ions are more densely packed in the near wall region in this case compared to case 1 (in fact, the average shortest distance between two Cl^- ions within 0.41 nm from the channel wall is found to be 0.54 nm for this case, and 0.69 nm for case 1), the electrostatic repulsion between ions is much stronger compared to case 1—hence, the second concentration peak is more distinct in this case.

The water concentration profile in Fig. 3 shows two interesting features. First, compared to the previous case [see Fig. 2(a)], the first concentration peak of water is about 33% higher. Second, there is an additional water concentration peak located at about 0.44 nm away from the channel wall and the second concentration peak is very close to the second peak of the Cl^- concentration. This result indicates that under high surface charge density, the high concentration of ions near the channel wall can change the concentration of water significantly. Such a change can be partly explained by the hydration of the ions. Typically there will be several water molecules bound to each ion due to the strong charge-dipole interaction between the ion and water.[15] Therefore, a region with very high ion concentration tends to have a high water concentration region near it.

Figure 4 shows the Na^+ ion concentration profile across the channel for case 3, where the channel width is 3.49 nm and the charge density on the channel wall is -0.120 C/m^2. The only difference from the first case is that the wall is oppositely charged and the Cl^- ions are replaced by Na^+ ions. We observe that (1) the first Na^+ concentration peak near the wall is about 37% lower compared to the Cl^- concentration peak in the first case, (2) the position of the first peak is located at about 0.42 nm away from the channel wall, i.e., about 0.07 nm farther away from the channel wall compared to the first case where the first Cl^- ion peak is located at 0.35 nm away from the channel wall and (3) the second Na^+ ion concentration peak is much more distinct compared to case 1. The first ion concentration peak is lower in this case because the attractive interaction between the Na^+ ion and the Si wall atoms—which contributes significantly to the high ion concentration near the channel wall—is much weaker compared to the Cl^- ion with the Si wall atoms (see Table I). The second observation can be explained by the fact that though Na^+ ion (bare radius about 0.095 nm) is smaller compared to the Cl^- ion, its hydrated radius (0.36 nm) is bigger compared to the Cl^- ion (0.33 nm) as Na^+ ion can attract more water molecules around it (the hydration number of Na^+ ion is about 4–5 while the hydration number of Cl^- ion is about 1).[15]

The second Na^+ concentration peak is primarily caused by the ion–water interactions. Figure 4 indicates that the second ion concentration peak is close to the second concentration valley of water. As explained in case 1, such a water concentration valley is energetically more favorable than the bulk for ions. Since the bare ion radius of Na^+ is much smaller compared to the Cl^- ion, the Na^+ ion can fit into the water concentration valley more easily compared to the Cl^- ion. Therefore, the second concentration peak of Na^+ ion is more distinct compared to the Cl^- ion case. One consequence of the higher second peak of Na^+ ion is that the water concentration valley near the second Na^+ peak is shallower compared to that observed in the Cl^- ion case (case 1). This is because the Na^+ ion has a higher hydration number. Thus, it can bring more water molecules towards the water concentration valley than the Cl^- ion.

B. Modified Poisson–Boltzmann equation

In Sec. IV A we have shown that the wall–ion, water–ion, and ion–ion interactions are important factors influencing the ion distribution in the channel and the ion distribution can significantly influence the water concentration in the channel. The classical Poisson–Boltzmann equation considers these interactions only in a mean-field fashion and fails to account for the molecular nature of the ion, water and the wall (e.g., water is modeled as a continuum with a constant permittivity). In this section, we propose a modified Poisson–Boltzmann equation that takes into account the wall–ion, water–ion, and ion–ion interactions in a lumped manner. The Poisson–Boltzmann equation has been modified previously to incorporate various effects that were neglected in the classical Poisson–Boltzmann equation, e.g., the finite ion size effects,[32] nonelectrostatic interactions,[33] dependence of the permittivity of the solution on the field strength,[34] wall effects,[35] and more recently discrete solvent effects[36] have

been incorporated into the classical Poisson–Boltzmann equation. Many of these modifications were based on statistical mechanics principles, and by incorporating all these effects into the Poisson–Boltzmann equation, it is possible to predict the ion distribution in the channel with good accuracy. However, due to the extremely complicated nature of the ion–wall, ion–water, and ion–ion interactions, a number of simplifications need to be made in the derivation of the modified Poisson–Boltzmann equation and the calculation of the new terms can still be very difficult in many cases. For example, though the wall–ion interaction is considered in Ref. 35, it was not discussed how such a term can be computed in practice (in fact, this term is usually neglected in numerical simulations[37]). Thus, though these existing modifications to the Poisson–Boltzmann equation can aid in the interpretation of various experimental observations, the development of a comprehensive, easy-to-calibrate and accurate model is still an active area of research.

In this paper, we employ the concept of electrochemical potential correction to account for the interactions neglected in the classical Poisson–Boltzmann equation. At thermodynamic equilibrium, the electrochemical potential of an ion should be constant in the entire system, i.e.,

$$\mu_i = \tilde{z}_i q \psi + k_B T \log c_i + \phi_{ex,i} = k_B T \log c_{0,i}, \tag{5}$$

where $\tilde{z}_i$ is the valency of ion i, ψ is the electric potential in the system, c_i is the ion concentration, $\phi_{ex,i}$ is the electrochemical potential correction of ion i, and $c_{0,i}$ is the concentration of ion i when the electric potential and the electrochemical potential correction term are zero. Based on Eq. (5), the ion concentration can be expressed as

$$c_i = c_{0,i} e^{-\tilde{z}_i q \psi / k_B T} e^{-\phi_{ex,i}/k_B T}. \tag{6}$$

Substituting Eq. (6) into the Poisson equation (7), we have

$$\nabla^2 \psi = -\frac{q}{\epsilon} \sum_{i=1}^{N} \tilde{z}_i c_i, \tag{7}$$

$$\nabla^2 \psi = -\frac{q}{\epsilon} \sum_{i=1}^{N} \tilde{z}_i c_{0,i} e^{-\tilde{z}_i q \psi / k_B T} e^{-\phi_{ex,i}/k_B T}, \tag{8}$$

where N is the total number of ionic species and is equal to 1 in all our simulations.

The electrochemical potential correction term accounts for the deviation of the ion–water and ion–wall molecular interactions from their values at the channel center. Since the wall–ion interaction via the Lennard-Jones potential is short-ranged, and the water–ion interaction would not deviate significantly in the entire system except at positions very close to the channel wall where the water concentration is not constant, the electrochemical potential correction term is nonzero only at positions close to the channel wall. The precise contribution of ion–water and ion–wall molecular interactions to the electrochemical potential correction term depends on the specific case under study. For example, for case 1, where the ion–wall ($Cl^- - Si$) interaction is strong, the contribution of the ion–wall molecular interactions to the electrochemical potential correction term is significant, whereas for case 3 the contribution of ion–wall ($Na^+ - Si$) molecular interactions will be minor.

In principle, one can calculate ϕ_{ex} provided the wall–ion, water–ion, and ion–ion interactions can be computed explicitly. However, such a calculation, if possible, is very difficult. For example, to account for the molecular nature of water, the charge–dipole interaction between water and the ion as well as other molecular interactions (e.g., the van der Waals interaction as included in the Lennard-Jones potential) will need to be considered explicitly. In addition, since the water concentration profile in the channel is related to the ion concentration profile [as demonstrated by the correlation between the second peak of the ion concentration with the water concentration valley in Figs. 2(a), 3, and 4], the concentration profiles of water and the ion must be computed self-consistently.

In this paper, we extract the electrochemical potential correction, term from the ion concentration profile obtained from MD simulation of a smaller width channel using Eq. (6). Once the electrochemical potential correction term is obtained, one can use it in the modified Poisson–Boltzmann equation (8) to simulate the ion distribution in a bigger channel with the same wall structure and similar surface charge density. In such an approach, one circumvents the difficulty of obtaining a closed form expression for the electrochemical potential correction term by utilizing the MD simulation results.

The accuracy of this approach depends on how significantly the wall–ion and water–ion interactions near the wall change when the channel size and the operating conditions are different (e.g., wall charge density and the wall structure). In fact, if the operating conditions are similar, the interactions will not change significantly. This is because (1) the wall–ion interaction included in the electrochemical potential correction term is the Lennard-Jones potential which depends only on the wall structure and the Lennard-Jones parameters and thus will not change when the channel width is increased; (2) the water–ion interactions depend primarily on the water concentration (i.e., how closely the water molecules are packed). MD simulation results of water concentration profile in channels of different width but with the same surface charge density indicate that the water concentration profile near the channel wall is independent of the channel width. In summary, the electrochemical potential correction term is primarily due to the wall effects (e.g., ion–wall interactions and wall-induced water layering). As these interactions are short-ranged, further addition of water layers in the bulk (corresponding to a wider channel) would not affect the electrochemical potential correction term significantly. Hence, the use of the same electrochemical potential correction term for wider channels can produce reasonably accurate results.

The efficiency of this approach depends on how the MD simulation cost scales when the system size increases, i.e., the approach is only useful when the MD simulation of a smaller channel system can be carried out easily and the computational cost for MD simulation of a larger system is very expensive. This is indeed true since the MD simulation for a smaller channel system (e.g., a 2-nm-wide channel) can

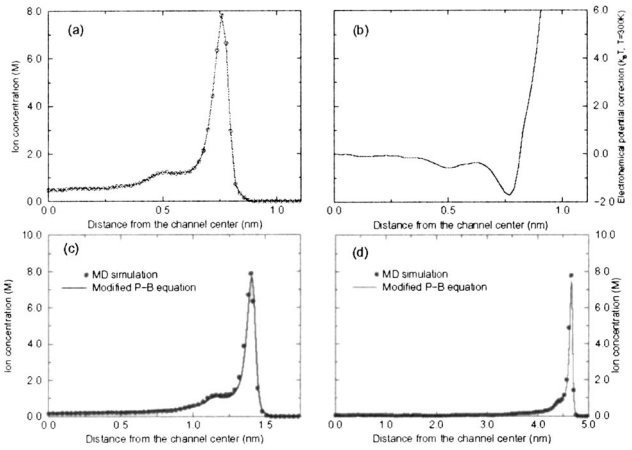

FIG. 5. (a) Cl^- ion concentration across the channel for case 4 ($W=2.22$ nm, $\sigma_s=+0.120$ C/m^2). (b) The electrochemical potential correction term extracted from the ion distribution shown in (a). (c) Comparison of Cl^- ion concentration across the channel for case 1 ($W=3.49$ nm, $\sigma_s=+0.120$ C/m^2) as predicted by the MD simulation and modified P–B equation. (d) Comparison of Cl^- ion concentration across the channel for case 6 ($W=10.0$ nm, $\sigma_s=+0.124$ C/m^2) as predicted by the MD simulation and modified P–B equation.

be done fairly quickly, while the MD simulation of larger system (e.g., a 6 nm wide channel) is much more expensive. Another good example for such a scenario is the nanofluidic system studied by Kemery *et al.*[3,11] where nanochannels are connected by microchannels. In this case, the MD simulation of the nanochannels is possible, but the MD simulation for the entire system is impossible.

Figure 5(a) shows the MD concentration profile of Cl^- ion across the channel for case 4, where the channel width is 2.22 nm and the surface charge density on the channel wall is 0.120 C/m^2. Figure 5(b) shows the electrochemical potential correction term extracted by using Eq. (6). Note that the electrochemical potential correction term is close to zero at about 0.8 nm away from the channel wall. ϕ_{ex} reaches a minima at about 0.34 nm away from the channel wall, and this roughly corresponds to the position of the minima of the potential energy due to the Lennard-Jones potential between the wall and the Cl^- ion [see Fig. 2(b)]. This indicates that the electrochemical potential correction term at this position is primarily due to the Lennard-Jones potential between the wall and the Cl^- ion. Using the electrochemical potential correction term shown in Fig. 5(b), the ion distribution in various channels with different widths and similar surface charge density were calculated. Figure 5(c) shows the comparison of Cl^- concentration in a 3.49 nm channel (case 1, charge density: 0.120 C/m^2) predicted by MD simulation and by the modified Poisson–Boltzmann equation. Figure 5(d) shows the comparison of Cl^- concentration in a 10.0 nm channel (case 6, charge density: 0.124 C/m^2) predicted by MD simulation and by the modified Poisson–Boltzmann equation. The results in Figs. 5(c) and 5(d) suggest that the modified Poisson–Boltzmann equation predicts the variation of the ion concentration near the channel wall very well in all the cases.

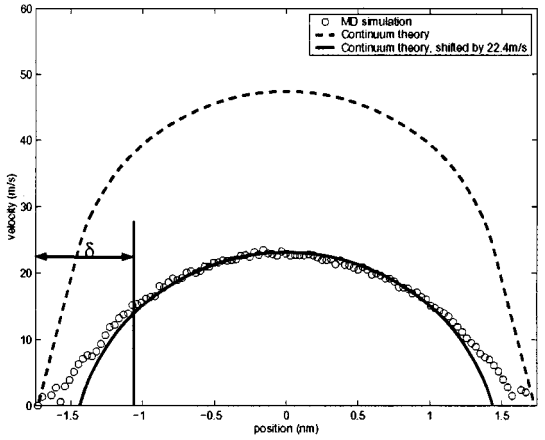

FIG. 6. Comparison of water velocity profile across the channel for case 1 ($W=3.49$ nm, $\sigma_s=+0.120$ C/m^2) as predicted by the MD simulation and by the continuum flow theory.

V. VELOCITY PROFILES IN ELECTROOSMOTIC FLOW

A. Comparison of continuum and MD simulation results

Figure 6 shows the velocity profile across the channel for case 1, where the channel width is 3.49 nm. The velocity profile based on the continuum flow theory, calculated by substituting the ion concentration obtained from the MD simulation into Eq. (2) and using the boundary condition specified by Eq. (4), is also shown for comparison.

Figure 6 shows that the continuum flow theory prediction using a constant viscosity of 0.743 mPa s overestimates the velocity in the entire channel. This is because the continuum calculation fails to take into account the fact that the viscosity near the channel wall is much higher compared to its bulk value. As has been reported earlier,[14] the viscosity of water increases dramatically in the near wall region where the ion concentration is high. Such a dramatic increase in viscosity seems to be related to the high electric field strength,[19] layering of the fluid molecules[38] and the high concentration of ions near the channel wall. However, a comprehensive theory accounting for all the effects is not yet available. The question of whether the continuum flow theory based on a constant viscosity can predict the flow behavior in the central part of the channel is an interesting one. We observe that, if the predicted velocity is shifted down by about 22.4 m/s, the continuum prediction matches the MD velocity at a distance of δ away from the channel wall, i.e., the continuum prediction matches the MD simulation result very well in the central portion of the channel. This is equivalent to saying that if the velocity at a position δ away from the channel wall is given as the boundary condition to the Stokes equation (2), then the continuum flow theory based on a constant viscosity can still be used to predict the velocity in the central part of the channel. Figure 6 also indicates that the nonslip boundary condition is applicable to the case studied. However, the nonslip plane is not located at the center-of-mass of the innermost layer of the channel walls (i.e., layer I in Fig. 1), but is located at approximately 0.14 nm from the channel wall where the water concentration is almost zero.

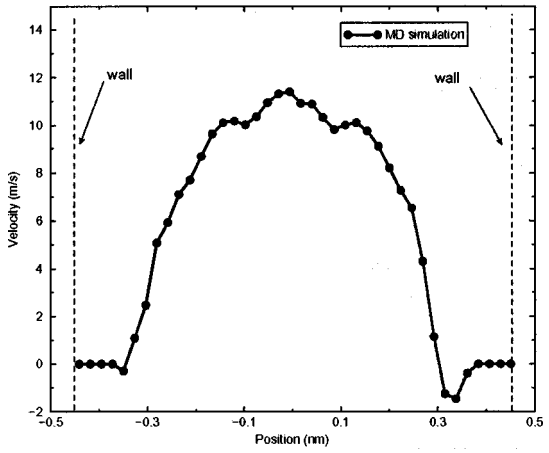

FIG. 7. Velocity profile across the channel for case 5 ($W=0.95$ nm, $\sigma_s=+0.124$ C/m^2). The negative velocity close to the channel wall is statistical noise.

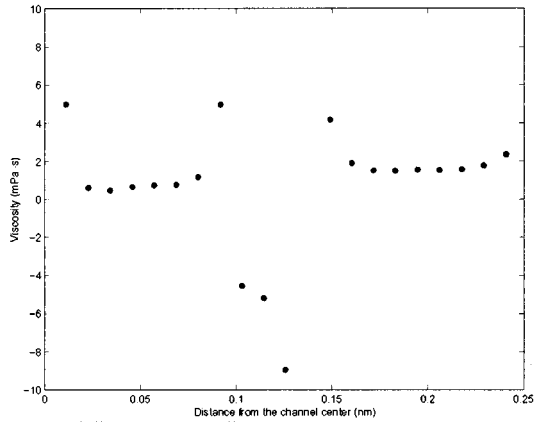

FIG. 8. Shear viscosity across the channel for case 5 ($W=0.95$ nm, $\sigma_s=+0.124$ C/m^2). Note that the shear viscosity, computed by using a linear, local constitutive relationship diverges at $|z|\approx 0.14$ nm and becomes negative in the region 0.09 nm$<|z|<0.14$ nm.

Comparison of velocity obtained from MD simulation and continuum flow theory for case 4, where the channel width is 2.22 nm, also indicates that though the continuum flow theory based on a constant viscosity overestimates the velocity in the entire channel, it can be used to study the flow behavior in the central part of the channel provided that the velocity at a position δ away from the channel wall is given. It is also observed that the nonslip plane is located at approximately 0.14 nm from the channel wall. This is similar to what Travis *et al.*[12] had observed for Poiseuille flow of Lennard-Jones atoms in various channel widths where the nonslip plane is located at the position closest to the channel wall that a fluid atom can approach and is independent of the channel width.

Figure 7 shows the velocity profile of water across the channel for case 5, where the channel width is 0.95 nm and the surface charge density is 0.124 C/m^2. The characteristics of the velocity profile are significantly different from that of case 1 (channel width: 3.49 nm) and case 4 (channel width: 2.22 nm). Specifically, (1) the strain rate du/dy goes to zero at $|z|\approx 0.09$ nm and $|z|\approx 0.14$ nm and (2) the velocity at $|z|\approx 0.14$ nm is higher compared to the velocity at $|z|\approx 0.09$ nm and the velocity decreases from $|z|\approx 0.14$ nm to $|z|\approx 0.09$ nm. Similar behavior was also observed by Travis *et al.*[12,39] for Poiseuille flow of Lennard-Jones atoms when the channel width approaches 4 to 5.1 times the diameter of the fluid molecules. This behavior suggests that the continuum flow theory is not valid for fluid flow in such narrow channels. Specifically, the velocity profile shown in Fig. 7 indicates that the shear stress cannot be related to the strain rate by a local, linear constitutive relationship. The shear stress across the channel can be computed by

$$\tau_{zx}(z)=\int_0^z c(z)\tilde{z}qE_{\mathrm{ext},x}\,dz, \tag{9}$$

where $z=0$ is the middle plane of the channel, $c(z)$ is the ion concentration and $E_{\mathrm{ext},x}$ is the external electric field along the channel length (x-direction). Figure 8 is a plot of the shear viscosity calculated by

$$\mu(z)=\frac{\tau_{zx}(z)}{du/dz|_z}. \tag{10}$$

Figure 8 indicates that the shear viscosity, computed by assuming a local, linear constitutive relationship between shear stress and strain rate, diverges at $z\approx\pm 0.14$ nm and $z\approx\pm 0.09$ nm, and becomes negative in the region 0.09 nm $<|z|<0.14$ nm. These unphysical results indicate that the continuum flow theory, which assumes that the shear stress can be related to the strain rate by a local constitutive relationship, is not valid for electroosmotic flow in a 0.95 nm wide channel.

B. Embedding MD velocity into continuum modeling

The results in Sec. V A indicate that the continuum flow theory is not valid for electroosmotic flow in a 0.95 nm wide channel. However, continuum theory can be used to describe flow in channels wider than 2.22 nm, provided that viscosity variation near the channel wall is taken into account. It is, however, very difficult to obtain a closed form expression for viscosity variation near the channel wall. To simulate electroosmotic flow in wide channels, where MD simulation can be very expensive, one possible way is to first do an MD simulation in a smaller channel under similar conditions (e.g., using the same wall structure and charge density as a wider channel) and then extract the viscosity from the MD data by using Eqs. (9) and (10). The extracted viscosity can then be used in continuum theory to model flow in a wider channel. In this approach, one assumes that the viscosity near the channel wall would not change appreciably when the channel width increases. This assumption typically holds since viscosity depends on the fluid properties and ion concentrations near the channel wall, and these parameters would not change significantly when the channel width changes provided that other operating conditions (e.g., wall structure and wall charge density) do not change significantly or remain the same. The extraction of viscosity from molecular dynamics data using Eq. (10) can be difficult as one needs to compute the derivative of the velocity obtained from MD data. Since the velocity obtained from the MD simulation is

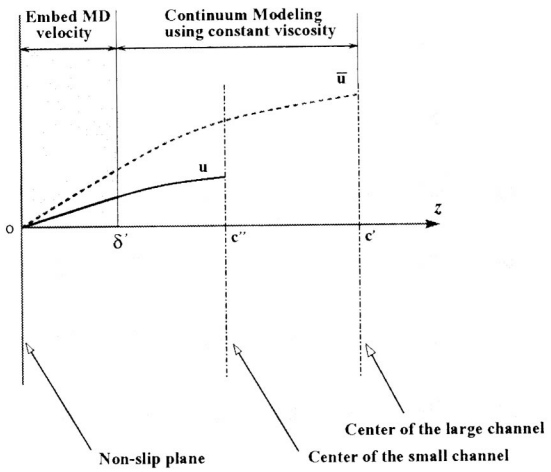

FIG. 9. Continuum simulation of electroosmotic flow in a large channel by using the velocity embedding technique. The channel is partitioned into two regions—a near wall region and a channel center region. The velocity near the wall is computed by embedding the velocity obtained from MD simulation of electroosmotic flow in a smaller channel. The velocity in the channel center region is computed by using the continuum flow theory based on a constant viscosity.

usually very noisy, unless the simulation is carried out for a relatively long period (e.g., case 4 has been simulated for 6.1 ns using about 200 CPU hours, but the statistical noise in the velocity profile near the channel wall is still observable), the derivative of the velocity would be even noisier leading to a significant noise in the extracted viscosity. It is possible to smooth the velocity data using a filter, but this may introduce additional errors into the viscosity estimation. An alternative approach is to embed the near wall velocity obtained from an MD simulation of a smaller channel into the continuum modeling of a larger channel. This approach is described below.

Figure 9 presents details on the simulation of electroosmotic flow in a large channel using the velocity obtained from MD simulation of electroosmotic flow in a small channel. For any position within δ' from the nonslip plane, the velocity in the large channel is obtained by embedding the MD velocity obtained for the electroosmotic flow in a small channel. Once the velocity at $z=\delta'$ is obtained, it is used as the boundary condition for the continuum flow modeling in the central portion of the large channel using a constant viscosity. To embed the small channel MD velocity u within δ' from the nonslip plane into the simulation of flow in a large channel, we first integrate the momentum equation (2) from the channel center (c'' is the center of small channel and c' is the center of the large channel) to a position z

$$\mu \left.\frac{du}{dz}\right|_{s=c''}^{z} = \int_{c''}^{z} -\tilde{z}qc(s)E_{\text{ext}}\,ds, \tag{11}$$

$$\mu \left.\frac{d\bar{u}}{dz}\right|_{s=c'}^{z} = \int_{c'}^{z} -\tilde{z}q\bar{c}(s)\bar{E}_{\text{ext}}\,ds, \tag{12}$$

where u, c, and E_{ext} are the velocity, the ion concentration and the external electric field at any position z in the small channel, respectively. $\bar{u}$, $\bar{c}$, and $\bar{E}_{\text{ext}}$ are the velocity, the ion concentration and the external electric field at any position z in the big channel, respectively. Using the symmetry of the velocity profile with respect to the channel center

$$\left.\frac{du}{dz}\right|_{s=c''} = \left.\frac{d\bar{u}}{dz}\right|_{s=c'} = 0. \tag{13}$$

Dividing Eq. (12) by Eq. (11) and applying Eq. (13) gives

$$\left.\frac{d\bar{u}}{dz}\right|_{z} = \frac{\int_{c'}^{z} -\tilde{z}q\bar{c}(s)\bar{E}_{\text{ext}}\,ds}{\int_{c''}^{z} -\tilde{z}qc(s)E_{\text{ext}}\,ds}\left.\frac{du}{dz}\right|_{z} = F(z)\left.\frac{du}{dz}\right|_{z}, \tag{14}$$

where $F(z)$ is defined by

$$F(z) = \frac{\int_{c'}^{z} -\tilde{z}q\bar{c}(s)\bar{E}_{\text{ext}}\,ds}{\int_{c''}^{z} -\tilde{z}qc(s)E_{\text{ext}}\,ds}. \tag{15}$$

Integrating Eq. (14) from the nonslip plane (i.e., $z=0$) to any position z, and using the fact that the velocity is zero at the nonslip plane, we obtain

$$\bar{u}(z) = \int_{s=0}^{z} F(s)\frac{du}{ds}\,ds = F(z)u(z) - \int_{0}^{z}\frac{dF(s)}{ds}u(s)ds. \tag{16}$$

Equation (16) can be used to compute the velocity near the channel wall in large channels. Note that no derivatives of the MD velocity in the small channel are needed. Instead, one needs to calculate the derivative of the function $F(z)$. $F(z)$ is obtained by integrating the ion concentration and it is much easier to obtain good statistics for ion concentrations in MD simulations. In principle, Eq. (16) can be applied in the region from the nonslip plane to the center of the small channel (i.e., point c'' in Fig. 9). However, Eq. (16) is used only in the region within δ' from the channel wall. There are two reasons for this: First, evaluation of the function $F(z)$ is difficult as we approach the center of the small channel because the integration term in the denominator is close to zero. Second, since the viscosity variation is important only near the channel wall, we can use a constant viscosity in the region δ' away from the nonslip plane instead of embedding the MD velocity. In our simulations, δ' is taken to be 0.64 nm since MD simulations indicate that the viscosity variation beyond this length scale is small. As mentioned earlier, the nonslip plane is typically located at 0.14 nm from the channel wall. Hence, the region in which the velocity is obtained from the embedding technique is $\delta=0.78$ nm from the channel wall for the larger channel.

Figure 10 shows the velocity profile across a 10.0 nm channel (case 6) obtained by using the approach just described. The velocity within the δ distance from the channel wall is embedded using Eq. (16) and the MD velocity of a 2.22 nm channel. The velocity in the central portion of the channel is computed by using a constant viscosity of 0.743 mPa s. Though there is considerable noise in the MD velocity profile for case 4 (i.e., in the MD velocity of a 2.22 nm channel), the velocity obtained by using Eq. (16) matches the MD simulation results quite well.

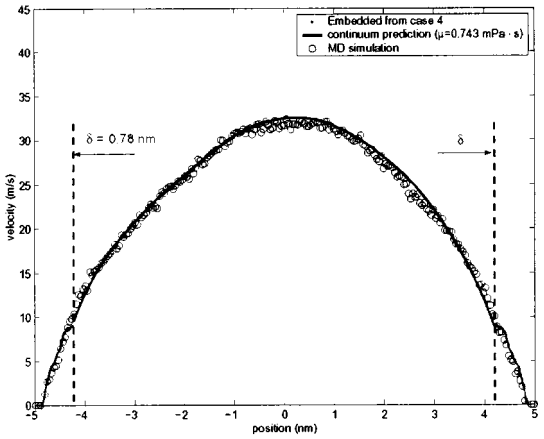

FIG. 10. Velocity profile across the channel for case 6 ($W=10.00$ nm, $\sigma_s=+0.124$ C/m^2). The velocity in the region within δ from the channel wall is obtained using Eq. (16) and the MD velocity within the same region from case 4 ($W=2.22$ nm, $\sigma_s=+0.120$ C/m^2). The velocity in the central portion of the channel is computed by using a constant viscosity of 0.743 mPa s.

VI. CONCLUSIONS

Electroosmotic flow in nanochannels with widths ranging from 0.95 to 10.00 nm has been investigated by MD and continuum simulations. Our results indicate that:

(1) For the various cases studied in this paper, the finite size of the ions and the discreteness of the solvent molecules have been found to significantly influence the ion distribution in the channel. Since the classical Poisson–Boltzmann equation neglects these effects, it fails to predict the ion distribution near the channel wall accurately. A modified Poisson–Boltzmann equation is proposed to account for the molecular aspects of the ion–wall, ion–fluid, and ion–ion interactions by introducing an electrochemical potential correction term into the formulation of the Poisson–Boltzmann equation. The electrochemical potential correction term is extracted from the ion distribution in a smaller channel obtained from MD simulations. Using the electrochemical potential correction term, the modified Poisson–Boltzmann equation has been shown to predict the ion distribution in nanometer wide channels with good accuracy.

(2) The continuum flow theory can be used to analyze electroosmotic flow in channels as small as 2.22 nm provided that the viscosity variation near the channel wall is taken into account. Instead of extracting viscosity near the channel wall from MD simulations, we have developed a technique where MD velocity from a smaller length scale channel is embedded into a larger length scale channel to compute velocity near the channel wall. We have shown that this technique gives good results when MD velocity from a 2.22 nm channel is embedded into simulation of larger channels with widths of 3.49 and 10 nm.

(3) The continuum flow theory breaks down in the entire channel for electroosmotic flow in a 0.95 nm channel (this channel width is about 3.4 times the size of the water molecule).

ACKNOWLEDGMENT

This research is funded by National Science Foundation under Grant Nos. ECS-0140496 and CCR-0121616. R.Q. is partially supported by a fellowship from the Center for Nanoscience and Technology (CNST) at the University of Illinois at Urbana-Champaign. The authors thank Zhi Tang for the silicon structure file and Sony Joseph for many helpful discussions.

[1] D. Harrison, K. Fluri, Z. Fan, C. Effenhauser, and A. Manz, Science **261**, 895 (1993).
[2] D. Reyes, D. Iossifidis, P. Auroux, and A. Manz, Anal. Chem. **74**, 2623 (2002).
[3] P. Kemery, J. Steehler, and P. Bohn, Langmuir **14**, 2884 (1998).
[4] A. Lehmani, O. Bernard, and P. Turq, J. Stat. Phys. **89**, 379 (1997).
[5] M. Eikerling, Y. Kharkats, A. Kornyshev, and Y. Volfkovich, J. Electrochem. Soc. **145**, 2684 (1998).
[6] R. Probstein, *Physicochemical Hydrodynamics* (Wiley, New York, 1994).
[7] L. Hu, D. Harrison, and J. H. Masliyah, J. Colloid Interface Sci. **215**, 300 (1999).
[8] N. A. Patankar and H. H. Hu, Anal. Chem. **70**, 1870 (1998).
[9] S. V. Ermakov, S. C. Jacobson, and J. M. Ramsey, Anal. Chem. **70**, 4494 (1998).
[10] M. Mitchell, R. Qiao, and N. Aluru, J. MEMS. **9**, 435 (2000).
[11] T. Kuo, L. Sloan, J. Sweedler, and P. Bohn, Langmuir **17**, 6298 (2001).
[12] K. Travis and K. Gubbins, J. Chem. Phys. **112**, 1984 (2000).
[13] L. Cheng, P. Fenter, K. Nagy, M. Schlegel, and N. Sturchio, Phys. Rev. Lett. **87**, 156103 (2001).
[14] J. Freund, J. Chem. Phys. **116**, 2194 (2002).
[15] J. Israelachvili, *Intermolecular and Surface Forces* (Academic, New York, 1992).
[16] M. Eikerling and A. Kornyshev, J. Electroanal. Chem. **502**, 1 (2001).
[17] D. van der Spoel, P. van Maaren, and H. Berendsen, J. Chem. Phys. **108**, 10220 (1998).
[18] A. Guzman-Garcia, P. N. Pintauro, M. W. Verbrugge, and R. F. Hill, AIChE J. **36**, 1061 (1990).
[19] R. Hunter, *Zeta Potential in Colloid Science: Principles and Applications* (Academic, London, 1981).
[20] P. Cummings and J. T. L. Varner, J. Chem. Phys. **89**, 6391 (1989).
[21] D. R. Lide and H. R. Frederikse, *CRC Handbook of Chemistry and Physics*, 19th ed. (CRC, Cleveland, 1998).
[22] H. Berendsen, J. Grigera, and T. Straatsma, J. Phys. Chem. **91**, 6269 (1987).
[23] *Gromacs User Manual Version 3.0*, Nijenborgh 4, 9747 AG Groningen, The Netherlands, Internet: http://www.gromacs.org (2001).
[24] W. Lo, K. Chan, M. Le, and K. Mok, J. Electroanal. Chem. **450**, 265 (1998).
[25] E. Lindahl, B. Hess, and D. van der Spoel, J. Mol. Model. [Electronic Publication] **7**, 306 (2001).
[26] H. J. C. Berendsen, D. van der Spoel, and R. van Drunen, Comput. Phys. Commun. **91**, 43 (1995).
[27] T. Darden, D. York, and L. Pedersen, J. Chem. Phys. **98**, 10089 (1993).
[28] I. Yeh and M. Berkowitz, J. Chem. Phys. **111**, 3155 (1999).
[29] B. Hess, H. Bekker, H. Berendsen, and J. Fraaije, J. Comput. Chem. **18**, 1463 (1997).
[30] M. Allen and D. Tildesley, *Computer Simulations of Liquids* (Oxford University Press, New York, 1987).
[31] H. Poppe, A. Cifuentes, and W. Kok, Anal. Chem. **68**, 888 (1996).
[32] I. Borukhov, D. Andelman, and H. Orland, Electrochim. Acta **46**, 221 (2000).
[33] L. Lue, N. Zoeller, and D. Blankschtein, Langmuir **15**, 3726 (1999).
[34] S. Woelki and H. Kohler, Chem. Phys. **261**, 411 (2000).
[35] Z. Adamczyk and P. Warszynski, Adv. Colloid Interface Sci. **63**, 41 (1996).
[36] Y. Burak and D. Andelman, J. Chem. Phys. **114**, 3271 (2001).
[37] Z. Wang, X. Yi, G. Li, D. Guan, and A. Lou, Chem. Phys. **274**, 57 (2001).
[38] J. Lyklema, S. Rovillard, and J. Coninck, Langmuir **14**, 5659 (1998).
[39] K. Travis, B. Todd, and D. Evans, Phys. Rev. E **55**, 4288 (1997).